Investigating the impact and reaction pathway of toluene on a SOFC running on syngas.

Tygue S. Doyle[a,*], Zahir Dehouche[a], P.V. Aravind[b], Ming Liu[b,*], Sinisa Stankovic[c]

[a] Centre for Energy and Built Environment Research, Brunel University, London UB8 3PH, UK
[b] Energy Technology Section, Delft University of Technology, Leeghwaterstraat 44, 2628 CA Delft, The Netherlands
[c] ChapmanBDSP, Saffron House, 6-10 Kirby Street, London EC1N 8TS, UK
* Corresponding authors: email: Tygue.Doyle@brunel.ac.uk, tel: +44 (0) 207618 4800; email: Ming.Liu@tudelft.nl

Abstract

The integration of solid oxide fuel cells (SOFCs) with gasification systems have theoretically been shown to have a great potential to provide highly efficient distributed generation energy systems that can be fuelled by biomass including municipal solid waste. The syngas produced from the gasification of carbonaceous material is rich in hydrogen, carbon monoxide and methane that can fuel SOFCs. However, other constituents such as tar can cause catalyst deactivation, and blockage of the diffusion pathways. This work examines the impact of increasing concentrations of toluene as a model tar in a typical syngas composition fed to a NiO-GDC/TZ3Y/8YSZ/LSM-LSM SOFC membrane electrode assembly operating at 850°C and atmospheric pressure. Results suggest that up to 20 g/Nm^3 of toluene and a low fuel utilisation factor (c.a. 17%) does not negatively impact cell performance and rather acts to increase the available hydrogen by undergoing reformation. At these conditions carbon deposition does occur, detected through EDS analysis, but serves to decrease the ASR rather than degrade the cell.

Alternatively, the cell operating with 32 g/Nm^3 toluene and with a fuel utilisation of 66.7% is dramatically affected through increased ASR which is assumed to be caused by increased carbon deposition. In order to test for the presence of tar products at the anode exhaust samples have been captured using an absorbing filter with results from HS-GC/MS analysis showing the presence of toluene only.

Nomenclature

F	Faraday constant [C/mol]
$\dot{n}$	molar flow rate [mol/s]
P	Pressure [kPa]
T	Temperature [°C]
U_f	utilisation factor [-]
x_i	molar fraction [-]
ASR	Area Specific Resistance
EDS	Energy Dispersive Spectrometer
GDC	Gadolinium doped Ceria
HS-GC/MS	Headspace Gas Chromatography/Mass Spectrometry
LSM	Lanthanum Strontium Manganese Oxide
TZ3Y	3mol% Y_2O_3 doped ZrO_2
8YSZ	8mol% Y_2O_3 doped ZrO_2
	Antoine Coefficients
A	13.932
B	3056.97
C	217.625

Keywords: SOFC, syngas, model tar, carbon deposition

1. Introduction

The driving need to diversify and improve the global energy market is obvious and extensively discussed, and within this change fuel cell technology is widely regarded to have the potential to meet many of the demands of a sustainable future. High temperature SOFCs, which operate up to temperatures of 1000°C, are electrochemical engines with distinct advantages as well as challenges. Whilst these high temperatures are required to maximise the ion conductivity of the electrolyte they also provide advantages of fuel flexibility and the availability of high grade heat that can be used in combined heat and power (CHP) systems. Already there are commercial small scale residential systems operating on the existing natural gas infrastructure which have an electrical efficiency of 60% and a total CHP efficiency of 85% (*CFCL, 2009*). In these systems methane (CH_4) is steam reformed into hydrogen (H_2) and carbon monoxide (CO)(Eq. 1) which can be further converted to carbon dioxide (CO_2) and more H_2 through a water gas shift (WGS)(Eq. 3) or can be used as a fuel itself (Eq. 9). In order to initiate these reactions steam which is produced at the anode is recirculated from the exhaust to the incoming fuel and the exothermic reactions (Eqs.(5) and(7)) at the electrode is used to supply the endothermic reforming reaction.

$\Delta H^0 = 206\ \mathrm{kJ.mol^{-1}}$	$CH_4 + H_2O \leftrightarrow CO + 3H_2$	Eq. 1
$\Delta H^0 = 869\ \mathrm{kJ.mol^{-1}}$	$C_7H_8 + 7H_2O \leftrightarrow 7CO + 11H_2$	Eq. 2
$\Delta H^0 = -41\ \mathrm{kJ.mol^{-1}}$	$CO + H_2O \leftrightarrow CO_2 + H_2$ **(WGS)**	Eq. 3
	$C_nH_m + nH_2O \leftrightarrow nCO + \left(n + \frac{m}{2}\right)H_2$	Eq. 4
$\Delta H^0 = -242\ \mathrm{kJ.mol^{-1}}$	$H_2 + O^{2-} \rightarrow H_2O + 2e^-$	Eq. 5
$\Delta H^0 = -111\ \mathrm{kJ.mol^{-1}}$	$C + O^{2-} \leftrightarrow CO + 2e^-$	Eq. 6
$\Delta H^0 = -283\ \mathrm{kJ.mol^{-1}}$	$CO + O^{2-} \leftrightarrow CO_2 + 2e^-$	Eq. 7
$\Delta H^0 = -3772\ \mathrm{kJ.mol^{-1}}$	$C_7H_8 + 9O^{2-} \leftrightarrow 7CO_2 + 4H_2O + 18e^-$	Eq. 8
	$C_xH_y + \left(\frac{y}{2} + 2x\right)O^{2-} \leftrightarrow \frac{y}{2}H_2O + xCO_2 + (y + 4x)e^-$	Eq. 9

Another source of hydrogen that has the potential to fuel a SOFC is synthesis gas or syngas derived from the gasification of carbonaceous material, often coal but also biomass and municipal solid waste (MSW). Syngas comprises mainly of CO, CO_2, and H_2 along with smaller concentrations of CH_4, steam (H_2O), nitrogen (N_2)(if air is used for gasification), and trace amounts of tar, volatile alkali metals, nitrogen compounds, sulphur compounds, chlorine compounds and particulates (*Coll et al, 2001, Higman and van der Burgt, 2003, Lorente, 2013*). The tolerance of SOFCs against many of these impurities is uncertain and remains a topic for continued research. This is further complicated as the concentration of these impurities can vary widely even between the same gasifier type and depends on factors such as; feedstock, feedstock size, moisture content, temperature, pressure, gasification agent, residence time and the presence of bed catalysts (E4Tech, 2009).

In terms of gasifier categories and the amount of tar products formed the general agreement is that updraft systems are the worst producing c.a.100g/Nm^3, fluidised bed systems are intermediate at c.a.10g/Nm^3, and the downdraft the best producing c.a.1g/Nm^3 (*Milne et al, 1998*). The formation of tar is a function of temperature, time, feedstock size, the gasification agent (O_2, steam), geometry, and mixing in the chamber which can cause a large disparity between the type of the system and the amounts mentioned. Also, methods for extraction and analysis of the tar products can cause misleading results as capturing the full array of tars with their various boiling points is a difficult task.

The general definition of a tar is reported in *Milne et al* (1998) as: "The organics, produced under thermal or partial-oxidation regimes (gasification) of any organic material, are called "tars" and are generally assumed to be largely aromatic."

The typical tar composition for a biomass gasifier is presented in Table 1 (Milne et al, 1998; Col et al, 2001; Singh et al, 2005, and Mermelstein et al, 2009).

Table 1: Typical tar composition from biomass gasification

Compound	Composition (wt %)
Benzene	37.9
Toluene	14.3
Other one-ring aromatic hydrocarbons	13.9
Naphthalene	9.6
Other two-ring aromatic hydrocarbons	7.8
Three-ring aromatic compounds	3.6
Four-ring aromatic compounds	0.8
Phenolic compounds	4.6
Heterocyclic compounds	6.5
Others	1.0

In order to test the performance of a SOFC running on tar-laden syngas a synthetic composition using a model tar can be used, as reported by Mermelstein et al (2010 and 2011) using benzene, Namioka et al (2011) and Ming et al (2013) using toluene, and Mermelstein (2009) using both benzene and toluene. Other studies using naphthalene have been reported by Aravind (2008) and Hauth (2011). Limited studies using real syngas having been carried out and reported in Hofmann (2007, 2008, 2009) which were undertaken within the EU project BioCellUS (Biomass fuel Cell Utility System), and real tar from a coal gasifier have also been presented by Lorente et al (2012, 2013). In Lorente (2012) real tar from a coal gasifier was compared against toluene, as a real tar versus a model tar assessment, and results illustrated that carbon deposition arising from toluene were greater than that of the real tar. Therefore the results derived from using toluene as a model tar could be regarded as an overestimation of the effects of the total carbon deposition.

The influence of anode material can also have a substantial effect on the tolerance of the fuel cell to contaminants (Finnerty et al, 2000; Zhu et al, 2003; Aravind et al, 2008; Lorente et al, 2013). In Lorente *et al* (2013) test conducted using model and real tars on Ni/YSZ and Ni/GDC anode materials illustrated that the Ni/GDC material performed better than the conventional Ni/YSZ anode material and supports the argument that Ceria-based materials are more effective in suppressing carbon formation (Zhu et al, 2003). This resistance to carbon formation can also be explained by the influence of Ceria on the Nickel catalyst. Ceria serves to reduce the NiO crystallite size whilst increasing the metal dispersion which results in higher oxygen mobility and improved reducibility (Koo et al, 2014; Yong-zhao et al, 2013, Daza et al, 2009). For this reason a cell purchased from *H.C.Starck Ceramics GmbH* comprising of NiO-GDC/TZ3Y/8YSZ/LSM-LSM anode/electrolyte/cathode (double layer) has been used for these experiments.

The purpose of this research is to identify the conditions that would lead to carbon formation from the hydrocarbon species present in the syngas and how carbon deposition impacts the electrical performance of

the SOFC. Further analysis of the exhaust gas will be used to provide insight into the reaction pathway of the tar and the level of reformation occurring.

Previous studies have concluded that carbon deposition caused by the presence of tar at the anode can cause deactivation of the nickel catalyst whilst also restricting the diffusion pathways (*Liu et al, 2013, Lorente et al, 2012, Lee et al, 2012, Mermelstein et al, 2011*). Thereby impacting the electrical performance and can also cause irreversible damage to the cell. If allowed to condense these tar compounds can also build up inside pipework and fowl the gas flow (Mermelstein, 2011). Testing of the exhaust gas for the presence of volatile organic compounds (VOCs) will provide further understanding of the reaction pathway of the model tar, as there is a concern that the decomposition of the tar may lead to the growth of higher hydrocarbon molecules (Mermelstein, 2011).

1.1. Carbon formation pathways

Carbon forming reactions:

$\Delta H^0 = 75\ \text{kJ.mol}^{-1}$ $CH_4 \leftrightarrow C + 2H_2$ Eq. 10

$\Delta H^0 = 50\ \text{kJ.mol}^{-1}$ $C_7H_8 \leftrightarrow 7C + 4H_2$ Eq. 11

$\Delta H^0 = -173\ \text{kJ.mol}^{-1}$ $2CO \leftrightarrow C + CO_2$ **(Boudouard)** Eq. 12

$\Delta H^0 = -131\ \text{kJ.mol}^{-1}$ $CO + H_2 \leftrightarrow C + H_2O$ Eq. 13

The formation of carbon at the anode is directly related to the operating conditions of the cell and can be suppressed by employing a sufficiently high oxygen-to-carbon ratio which can be done by increasing the steam content at the inlet (this will promote steam reformation of the hydrocarbons, Eq. 1, 2 and 3), and/or by operating at sufficiently high current densities to ensure a large amount of oxygen ions are available to oxidise the carbon species (Eq. 5, 6, 7 and 8).

Temperature also plays an important role in carbon formation and there are a number of studies that use thermodynamic modelling to predict the potential for carbon formation, but as illustrated in Mermelsein (2011) and Lorente (2013) thermodynamic modelling should only be used as a guide as carbon has shown to form beyond predicted limits.

2. Experimental

2.1. Experimental Set-up

A square single cell SOFC test station has been modified to include the addition of a model tar by diverting nitrogen through a temperature controlled tar evaporator. The test station is equipped to supply the cell with a mixture of H_2, O_2, N_2, CO_2, CO, and CH_4 which are controlled using Bronkhorst Mass flow Controllers, and H_2O is supplied either through a Bronkhorst Controlled Evaporator Mixer (CEM) or a temperature controlled evaporator. Pipe work leading to the cell from the tar evaporator is trace heated to prevent condensation and the exit pipe coming from the anode is also trace heated to ensure none of the gases are able to condense prior to the first gas sampling point. After this sampling point the anode off-gas is bubbled through a condenser before passing through an absorber to eliminate any remaining moisture before a second gas sampling point which is connected to an Agilent Technologies 490 Micro GC. The ceramic cell housing is made from Al_2O_3 and is designed to provide a gas tight seal by using weights to apply pressure to

an appropriate gasket seal, in this case gaskets were cut from Termiculite® 866 mica. A platinum mesh spot welded to platinum wires is used to transfer current to the cathode and similarly a nickel mesh spot welded to platinum wires is used as a current collector at the anode. This housing is located in a furnace made up of ceramic insulating bricks. Further details of this setup can be found in Liu et al, 2013. In order to protect the cell from damage caused by excessive current, and also to avoid the risk of nickel oxidation, the experiments limit drawing current that pushes the voltage below 0.65V.

Table 2: Cell materials, characteristics and dimensions of the electrodes and electrolyte.

Cell material and geometry

Layer	Material description	Area dimensions (mm)	Thickness (μm)
Anode	Porous NiO/GDC	90 x 90	40 ± 10
Electrolyte	Dense TZ3Y	108 x 108	95 ± 15
Cathode	Porous 8YSZ/LSM-LSM double layer	90 x 90	40 ± 10

A current is drawn from the cell using an electrical load (PLZ603W Kikusui Electronics Corp.) with an additional compensation load (SM30-100D Delta Elektronika), which are connected in series with the cell. Electrochemical Impedance Spectroscopy (EIS) measurements and potential measurements are recorded using a Gamry Instruments FC350™ Fuel Cell Tester (FCI4™ interface) and works with the electrical load operated via a PC using Gamry Echem Analyst™ software. Thermocouples are placed throughout the test station measuring oven, cell, inlet and outlet tracing temperatures as well as the fluid temperatures in both the tar and water evaporators.

In order to control the amount of tar being added to the gas composition an evaporator using N_2 as a carrier gas was used. By controlling the flow rate of the carrier gas and the temperature of the evaporator the vapour pressure of a substance can be predicted using the Antoine equation.

$$\log_{10} P_{C_7H_8} = A - \frac{B}{T + C - 273.15} \quad \text{Eq. 14}$$

$$P_{C_7H_8} = x_{C_7H_8}.P_{evaporator} \quad \text{Eq. 15}$$

Here $P_{C_7H_8}$ and $P_{evaporator}$ represent the vapour pressure of the toluene and overall pressure inside the evaporator respectively, A, B, and C are the Antoine coefficients specific to toluene and T is the evaporator temperature, and $x_{C_7H_8}$ is the molar fraction of toluene.

Sampling of the untreated anode off-gas was taken using a 100ml syringe fitted with an absorbing filter to capture and test for any hydrocarbons that may be present at the exhaust. Filters were immediately frozen to preserve the contents before being tested for the presence of VOCs, tests were carried out by a commercial laboratory using Headspace Gas Chromatography/Mass Spectrometry (HS-GC/MS).

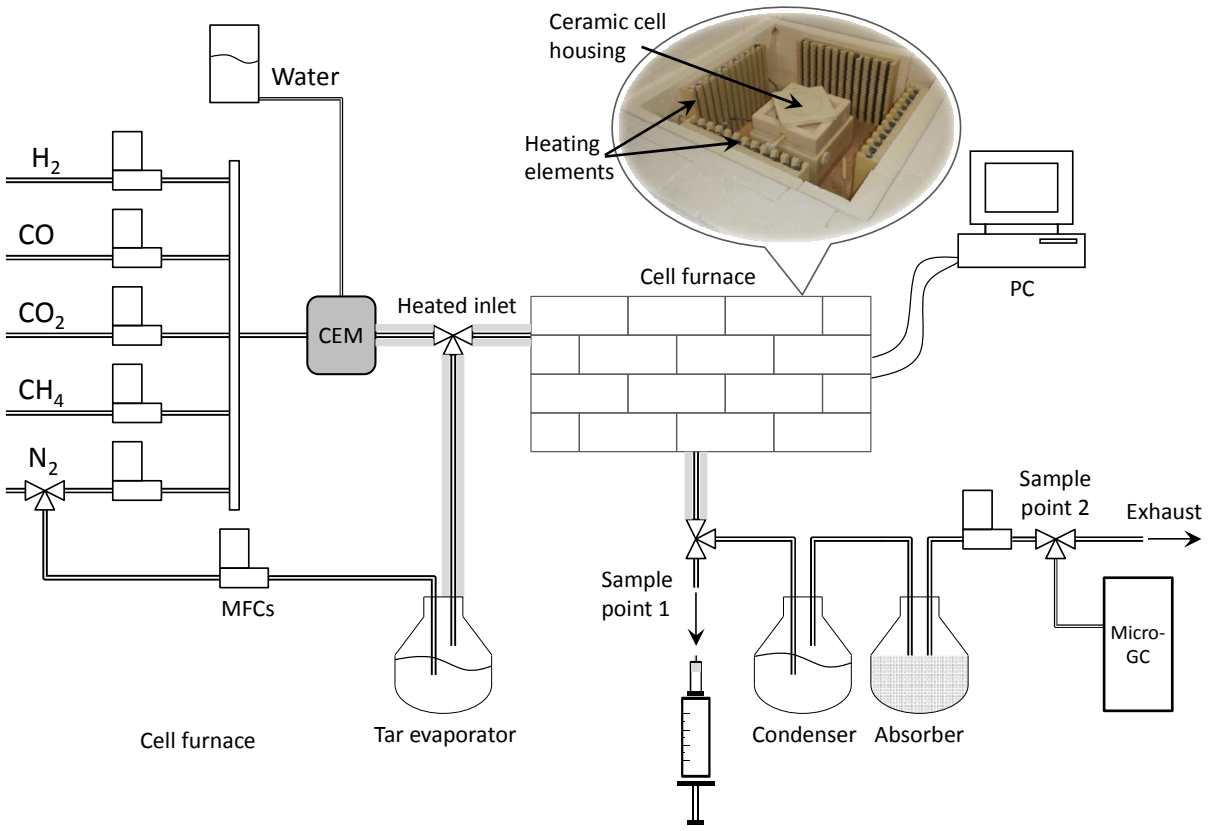

Figure 1: A schematic representation of the experimental setup.

2.2. Operating conditions

After the NiO at the anode was reduced Ni, using a mixture of H_2 and N_2, the cell was operated at a constant temperature of 850°C and at atmospheric pressure. The study included five variations in gas composition with the first four operating with a low fuel utilisation factor (U_f)(Eq. 16) and changes in the composition were specific to the tar, H_2O and N_2 concentrations. The variations in H_2O were to ensure the experiments were conducted with an oxygen-to-carbon ratio (O/C) of c.a. 1.8 which would protect the test station from carbon deposition in the pipework thereby preventing the need for costly repairs. The variation in N_2 was needed to ensure consistency in the volume fraction of the remaining gasses. The fifth experiment aimed to substantially increase the fuel utilisation factor whilst also increasing the tar concentration. The cathode was supplied with a mixture that represents a typical air composition of 320Nml/min O_2 and 1180 Nml/min N_2.

$$U_f = \frac{\mathrm{I}}{2F\dot{n}(x_{H_2} + x_{CO} + 4x_{CH_4} + 18x_{C_7H_8})} \qquad \text{Eq. 16}$$

Where I is current (A), F is the Faraday constant (C/mol), $\dot{n}$ is the total anode molar flow rate (mol/s), and x_i is the input molar fraction of the gas.

Table 3: Operating conditions of the five experiments undertaken indicating syngas composition and utilisation factor at 200 mA/cm^2 for each.

Experiment	1		2		3		4		5	
	Nml/min	vol %	Nml/min	vol %	Nml/min	vol %	Nml/min	vol %	Nml/min	vol %
H_2	306	28.2	306	27.9	306	27.9	306	27.9	77	29.0
CO_2	144	13.3	144	13.1	144	13.1	144	13.1	36	13.6
CO	286	26.3	286	26.1	286	26.1	286	26.1	72	27.1
N_2	119	11.0	115	10.5	97	8.9	60	5.4	13.9	5.2
CH_4	7.7	0.7	7.7	0.7	7.7	0.7	7.7	0.7	1.8	0.7
H_2O	10.8	g/hr	11.5	g/hr	12.3	g/hr	14	g/hr	3	g/hr
Toluene	0	g/Nm^3	5	g/Nm^3	10	g/Nm^3	20	g/Nm^3	32	g/Nm^3
U_f (@200 mA/cm^2)	18.1%		17.4%		16.8%		15.7%		66.7%	

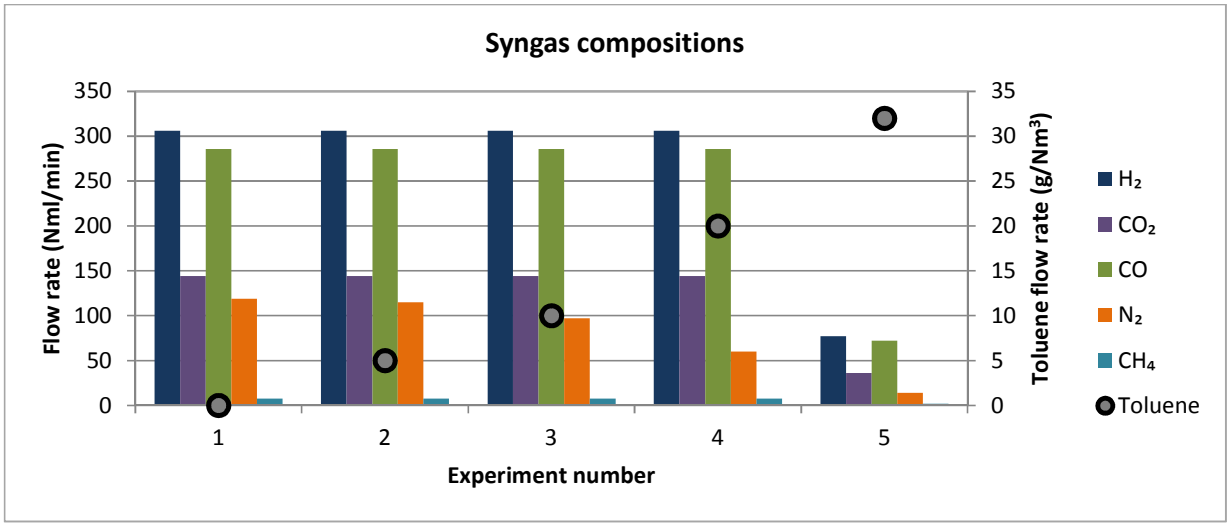

Figure 2: Graphical representation of gas composition indicating increasing levels of toluene concentration from 0 – 32 g/Nm^3.

2.3. Methodology

In order to measure the performance drop caused by the inclusion of the syngas reference measurements were taken prior to the introduction of any carbon species to the cell. For this purpose an I-V curve and EIS measurements were taken whilst supplying the cell with 400 Nml/min of H_2 and 800 Nml/min of N_2. EIS measurements were also taken after the completion of each experiment to record any changes to the cell's characteristics as a result of possible carbon deposition. For each experiment the gas composition at the exhaust was measured at open circuit voltage (OCV), 100 mA/cm^2 and again at 200 mA/cm^2 in order to track the changes to the CO and CO_2 flow rates which would indicate the level of reformation of the two hydrocarbon species and will give insight into the reaction pathways of the model tar. This was further assisted by capturing samples, at the first sampling point, using absorbing filters which have been tested for the presence of any tar products which would elucidate on the possibility of the initial hydrocarbons to break and reform into other hydrocarbon species. Also, to visualise and quantify the change in performance caused by the inclusion and removal of the model tar OCV readings were recorded for 10min before the

inclusion of the tar, then a further 30min with the tar added, and until the voltage stabilised after the tar was removed.

3. Results and discussion

3.1. OCV

The OCV, illustrated in *Figure 3*, of the reference experiment using just H_2 and N_2 at the anode is higher than that of the syngas experiments which is owed to the slightly higher partial pressure of H_2 and also due to the lack H_2O at the anode. Given the relatively consistent amounts of H_2 and H_2O the OCV of the syngas experiments are very similar and the fact that experiment 5 shows a slightly elevated OCV indicates that the high concentration of tar is undergoing reformation to increase the flow of H_2 (and hence the partial pressure). A localised drop in temperature caused by the endothermic reformation could also contribute to the increased voltage as temperature directly influences the Gibbs free enthalpy. Interestingly the gradient, which is an indication of the cells area specific resistance (ASR), is improved for experiments 1-4 illustrating improved cell performance under these conditions, even when compared to the carbon-free reference experiment. We can therefore postulate that small levels of carbon deposition can positively influence the electrical conductivity of the cell, but whether this can be maintained over a longer period remains to be answered. Experiment 5 demonstrates a visible increase in ASR which in this case could be a result of an over accumulation of carbon, which was confirmed by the EDS, at the anode.

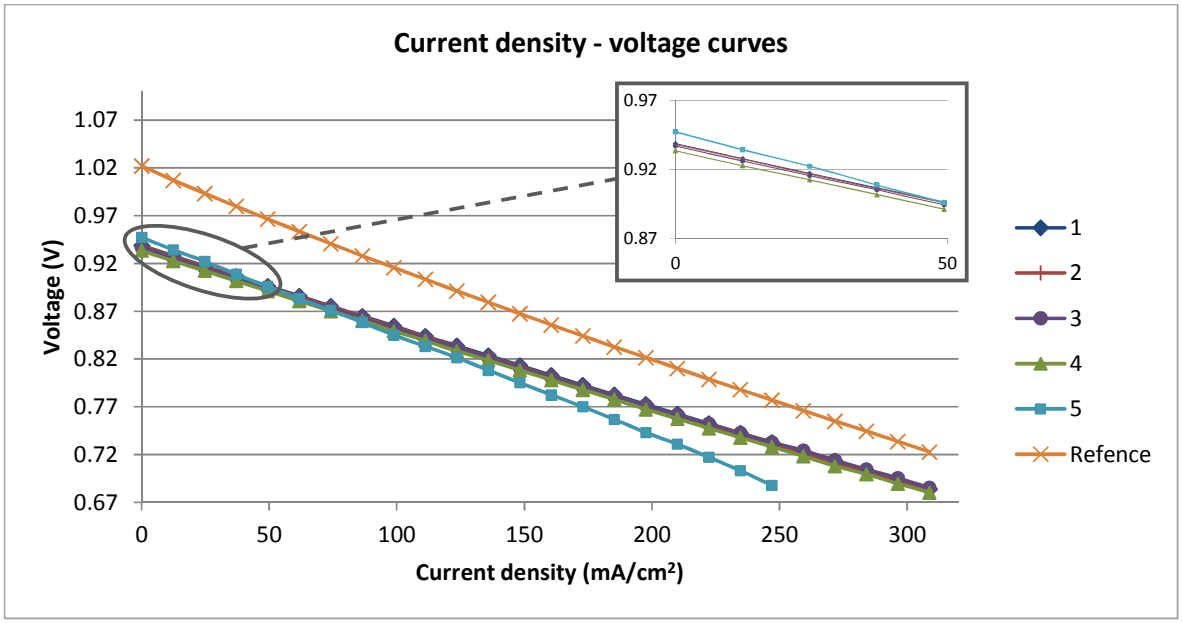

Figure 3: I-J curves for the five experiments undertaken along with a preliminary reference measurement taken for H_2/N_2 fuel mix with a similar H_2 partial pressure to the syngas experiments.

Results from monitoring the OCV at the inclusion, operation, and removal of the model, *Figure 4*, shows that at the inclusion of the tar the OCV increases (demonstrating more clearly that the tar is contributing to the amount of hydrogen available at the anode as a result of reformation) and remains constant for the 30min period. As mentioned the above, the endothermic reforming of the tar may also cause a localised drop in temperature which would contribute to the identified increase in OCV. This is explained by an increase in the Gibbs free enthalpy which varies with temperature and a drop in temperature would result in a slightly

increased OCV. Once the tar is removed we can see that the OCV recovers to its original level indicating no damage is caused from the introduction of tar to the fuel. These results were measured during experiment 4 (tar flow - 20 g/Nm^3).

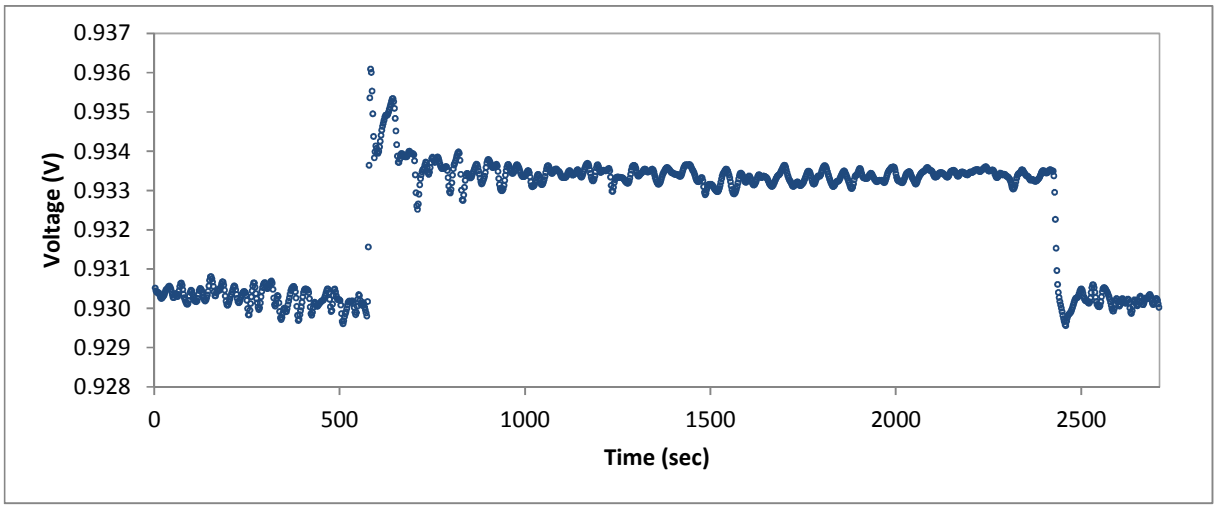

Figure 4: OCV measurements taken over time showing changes caused by the inclusion and removal of the tar species, taken during experiment 4.

3.2. EIS

Figure 5 presents the Nyquist plots of impedance and illustrates an ohmic resistance (defined by the *x* intercept in the high frequency region) of c.a. 0.7 Ω cm^2 for all experiments with a small increase in resistance for syngas experiments 1-5. The overall impedance for the cell in the reference experiment is c.a. 1.5 Ω cm^2, 1.4 Ω cm^2 for experiment 5, and c.a. 1.1 Ω cm^2 for experiments 1-4 which reflects the change in slope identified in *Figure 3*. The overall polarization (the difference between the ohmic resistance and overall impedance) for the reference experiment is c.a. 0.79 Ω cm^2, c.a. 0.64 Ω cm^2 for experiment 5, and c.a. 0.4 for experiments 1-4. It can be seen that for experiments 1-4 the impedance characteristics are not dissimilar even though the levels of tar are steadily increased and demonstrates no identifiable change to the structure of the material resulting from any possible carbon deposition. Experiment 5 is clearly adversely affected by the high tar concentration and the increased utilisation factor, which will influence the gas concentration along the surface of the anode thereby affecting the gas diffusion process, combined with the carbon deposition identified through SEM analysis we can conclude that these conditions are not suitable for this cell. The localised drop in temperature caused by the endothermic reforming of the hydrocarbon species in experiment 5 could further explain the increased overall impedance. An argument for decreased overall impedance for experiments 1-4 compared to the reference H_2/N_2 can be attributed to the participation of C and CO (*Eq. 6 and 7*) thereby reducing the polarization resistance by combining with the O^{2-} ions at the triple phase boundary. It is reasonable to conclude that if any carbon is being formed at the anode in experiments 1-4 there are little signs to show significant degradation. Results from energy dispersive spectrometer (EDS) presented in *Figure 7* illustrate the presence of carbon as a result of these experiments and with the evidence provided we can assume the conditions present in experiment 5 are most likely responsible. .

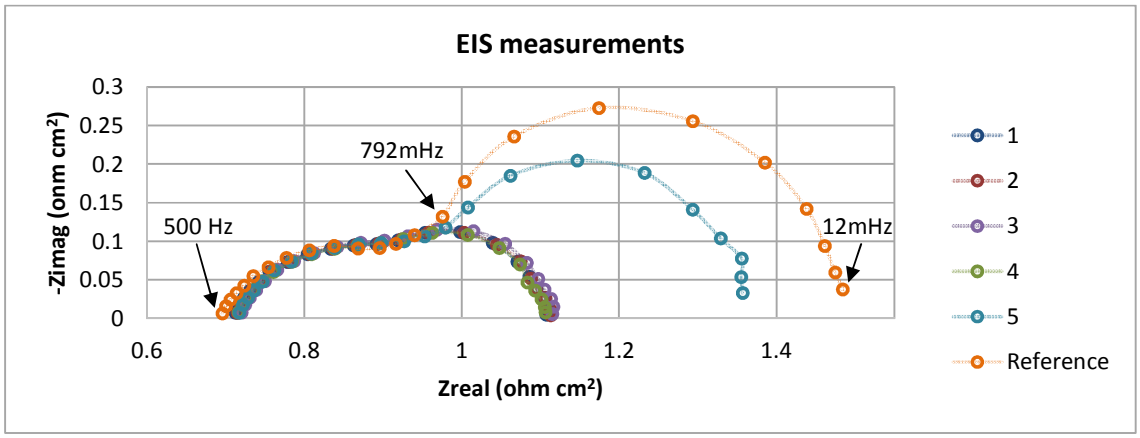

Figure 5: EIS measurements taken after each experiment to record changes to the cell as a result of exposure to increasing levels of tar, also compared to the initial H_2/N_2 reference experiment.

3.3. Exhaust gas analysis

By studying the trends in CO and CO_2 a t the exhaust we can see that the amount of CO_2 is substantially increased compared to the inlet which would be expected owing to the steam reforming of the CH_4 and C_7H_8 (toluene)(*Eq. 1 and 3*) to CO an d the shifting of CO to CO_2 through the WGS (*Eq. 2*). Hydrocarbon species can also undergo reformation straight to CO_2 without the WGS resulting in the same molar balance. The considerable amount of CO at the exhaust indicates the majority of the increase in CO_2 must result from the reformation of the hydrocarbon species. The gradual decrease in CO and CO_2 as the current density increases is an indication that there is either a fall in hydrocarbon reformation or, more likely, the production of solid carbon at the anode. Interestingly this trend increases even though the flux of oxygen ions at anode increases. As indicated and noted from the EIS measurements (*Figure 5*) the CO and CO_2 trends for experiment 5 indicate further carbon deposition which accounts for the substantial increase in the overall impedance and the drop in CO and CO_2 concentrations.

Results from the samples captured at the anode exhaust via the absorbing filters, shown in *Table 4*, show that the toluene model tar is still present at the exhaust and is the only tar product detected from the VOCs tested (the compounds tested and the limits of their detection are presented in *Table 4*). Even though the large array of hydrocarbon species tested is not exhaustive, these results begin to show that the reaction pathway of the toluene is to reform (Eq. 8) and not to combine into other hydrocarbon species. Whilst reformation is taking place results show that the tar is not completely reformed thereby leaving scope to optimise the conditions further to maximise the potential of the tar to fuel the SOFC. The trends for the VOC testing are not always consistent and may be a result of a number of factors that include; condensation at the sampling point, inconsistent drawing of the syringe, or insufficient protection of the filters during transportation.

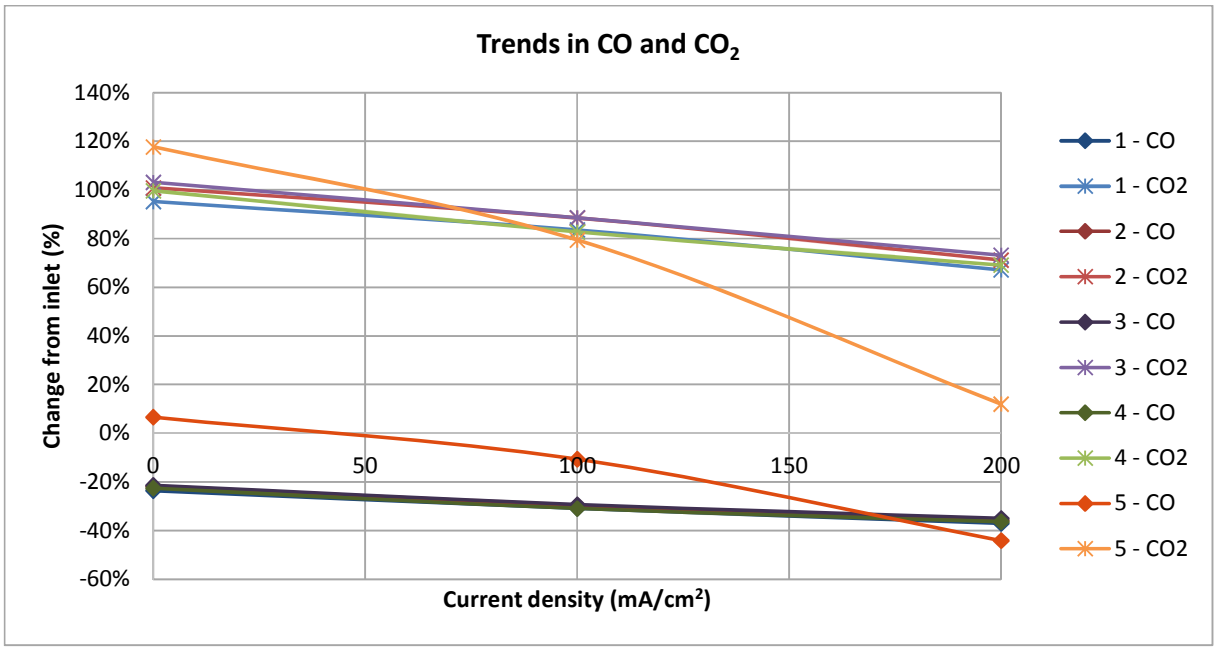

Figure 6: Graphical representation of the change in CO and CO_2 at the exhaust compared to the amount CO and CO_2 at the inlet measured at increasing current density.

Table 4: Third party HS-GC/MS analysis of samples captured via absorption filters at the anode exhaust. Tests were performed to detect the presence of VOCs and the list of compounds tested and the corresponding detection limits are shown. The only positive results came from the presence of toluene, all other compounds were not detected above the given detection limits.

Experiment			2			3			4			5		
	Unit	Limit of detection	0 mA/cm²	100 mA/cm²	200 mA/cm²	0 mA/cm2	100 mA/cm2	200 mA/cm2	0 mA/cm²	100 mA/cm²	200 mA/cm²	0 mA/cm²	100 mA/cm²	200 mA/cm²
Toluene	µg/kg	1	3.4	6.2	1.1	5.6	3.7	2.5	5.1	2.2	2.8	< 1.0	< 1.0	7.6

Other compounds tested with [Limit of detection in µg/kg]:
Chloromethane [4], Chloroethane [2], Bromomethane [6], Vinyl Chloride [24], Vinyl Chloride [24], Trichlorofluoromethane [5], 1,1-dichloroethene [7], 1,1,2-Trichloro 1,2,2-Trifluoroethane [7], Cis-1,2-dichloroethene [7], MTBE (Methyl Tertiary Butyl Ether) [1], 1,1-dichloroethane [6], 2,2-Dichloropropane [6], Trichloromethane [7], 1,1,1-Trichloroethane [7], 1,2-dichloroethane [4], 1,1-Dichloropropene [7], Trans-1,2-dichloroethene [7], Benzene [1], Tetrachloromethane [7], 1,2-dichloropropane [6], Trichloroethene [6], Dibromomethane [7], Bromodichloromethane [7], Cis-1,3-dichloropropene [7], Trans-1,3-dichloropropene [8], 1,1,2-Trichloroethane [5], 1,3-Dichloropropane [8], Dibromochloromethane [2], Tetrachloroethene [8], 1,2-Dibromoethane [3], Chlorobenzene [7], 1,1,1,2-Tetrachloroethane [4], Ethylbenzene [1], p & m-xylene [1], Styrene [5], Tribromomethane [7], o-xylene [1], 1,1,2,2-Tetrachloroethane [5], Isopropylbenzene [7], Bromobenzene [11], N-Propylbenzene [5], 2-Chlorotoluene [11], 4-Chlorotoluene [11], 1,3,5-Trimethylbenzene [4]. Tert-Butylbenzene [4], 1,2,4-Trimethylbenzene [5], Sec-Butylbenzene [5], 1,3-dichlorobenzene [7], P-Isopropyltoluene [16], 1,2-dichlorobenzene [5], 1,4-dichlorobenzene [8], Butylbenzene [4], 1,2-Dibromo-3-chloropropane [7], 1,2,4-Trichlorobenzene [9], Hexachlorobutadiene [7], 1,2,3-Trichlorobenzene [10].

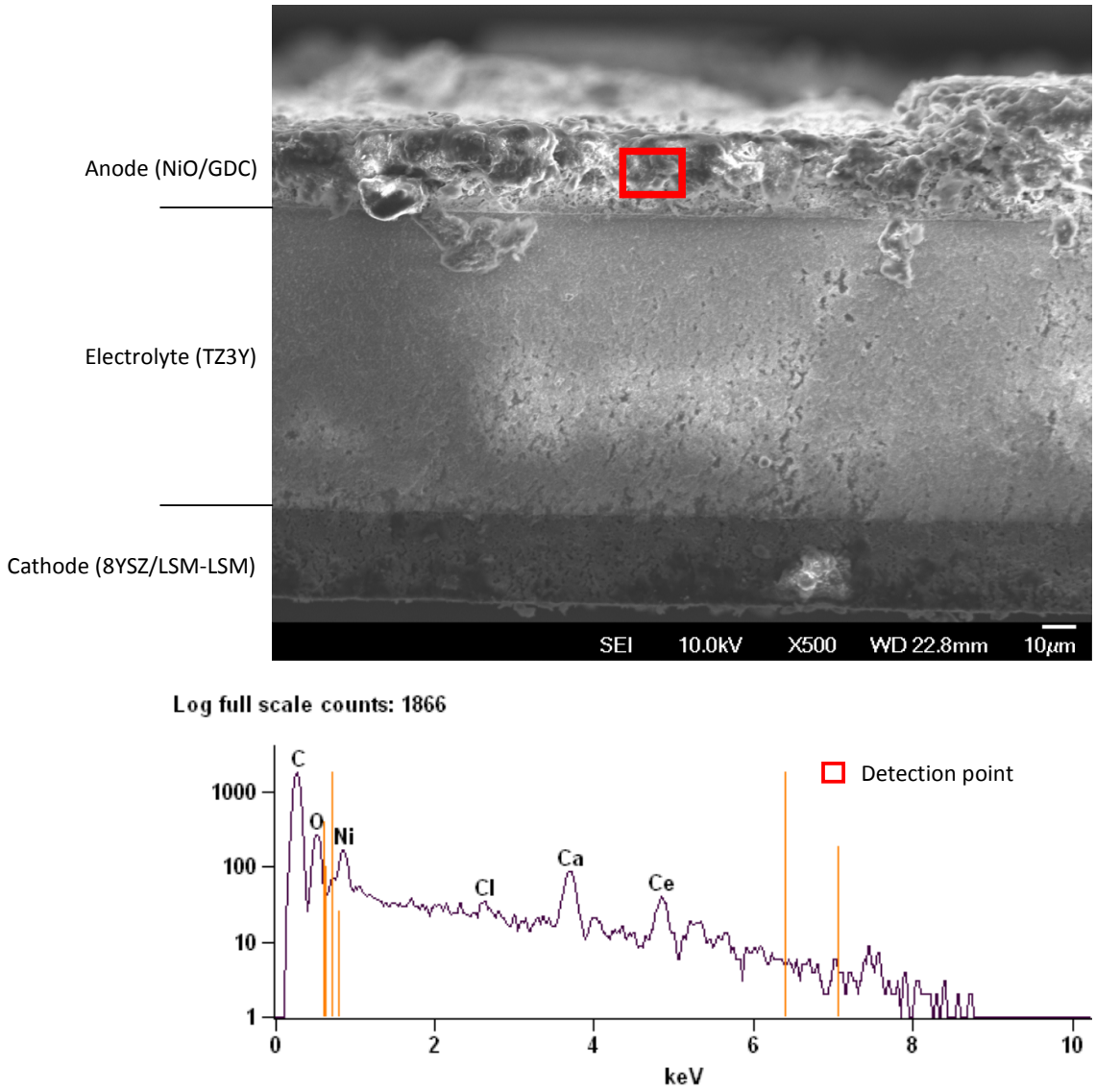

Figure 7: SEM image of a cross section of the cell illustrating the anode, electrolyte and cathode layers accompanied by an EDS analysis at the indicated region at the anode showing the presence of carbon.

4. Conclusions

From the experiments carried out we can conclude that the inclusion of toluene as a model tar, at concentrations that one would expect from a fluidised bed gasifier, have no immediate negative impact on the SOFC when using GDC as the anode material. Reasons contributing to this tolerance may include the low utilisation factor employed, the anode material used, as well as the controlled O/C ratio which was kept at c.a.1.8. Increasing the utilisation factor along with the tar concentration did however have a large impact on performance which from the results presented can be attributed to high levels of carbon formation and deposition at the anode. This is also supported by post experimental tests using scanning electron microscope (SEM) images and EDS analysis which show substantial levels of carbon deposition at the anode. Another important conclusion is shown by the VOC analysis at the exhaust that suggests whilst the model tar does undergo reformation that contributes to hydrogen production there is no evidence to suggest the formation of any other hydrocarbon species. The exhaust gas analysis shows that a certain amount of

toluene is still present, even under favourable SOFC conditions for the steam reforming, indicating that the conditions are yet to be optimized for better electrical performance.

5. Acknowledgements

The authors would like to thank the personnel at TU Delft for contributing with support and advice from the initial setup to analysing the final results. This research was funded in part by BRISK, a European Commission Capacities Project in the 7th Framework Programme, along with the Engineering and Physical Sciences Research Council in the UK.

6. References

Aravind P.V., Ouweltjes J.P., Woudstra N., Rietveld G., 2008. *Impact of biomass derived contaminants on SOFCs with Ni/Gadolinia-doped ceria anodes*. Electrochemical and Solid State Letters 11, B24-B28.

CFCL generator achieves 60% efficiency, Fuel Cells Bulletin, Volume 2009, Issue 4, ISSN 1464-2859.

Coll R., Salvado J., Farriol X., Montane D., 2001. *Steam reforming model compounds of biomass gasification tars: conversion at different operating conditions and tendency towards coke formation*. Fuel Processing Technology 74, 19-31.

Daza C.E., Kiennemann A., Moreno S., Molina R., 2009. *Dry reforming of methane using Ni–Ce catalysts supported on a modified mineral clay*. Applied Catalysis A: General 364, 65-74.

E4Tech, 2009. *Review of Technologies for Gasification of Biomass and Wastes: Final Report.* NNFC Project 09/008, June 2009.

Finnerty C.M., Ormerod R.M., 2000. *Internal reforming over nickel/zirconia anodes in SOFCs operating on methane: influence of anode formulation, pre-treatment and operating conditions*. Journal of Power Sources 86, 390-394.

Hauth M., Lerch W., Konig K., Karl J., 2011. *Impact of naphthalene on the performance of SOFCs during operation with synthetic wood gas*. Journal of Power Sources 196, 7144-7151.

Higman C., van der Burgt M., 2003. *Gasification*. Burlington, Elsevier Science.

Hofmann Ph., Panapoulos K.D, Aravind P.V., Siedlecki M., Schweiger A., Karl J., Ouweltjes J.P., Kakaras E., 2009. *Operation of solid oxide fuel on biomass product gas with tar levels > 10 h* Nm^{-3}. International Journal of Hydrogen Energy 34, 9203-9212.

Hofmann Ph., Panapoulos K.D, Fryda L., Schweiger A., Ouweltjes J.P., Karl J., 2007. *Integrating biomass gasification with solid oxide fuel cells: Effect of real product gas tars, fluctuations and particulates on Ni-GDC anode*. International Journal of Hydrogen Energy 33, 2834-2844.

Hofmann Ph., Schweiger A., Fryda L., Panapoulos K.D, Hohenwarter U., Siedlecki M., Bentzen J.D., Ouweltjes J.P., Ahrenfeldt J., Henriksen U., Kakaras E., 2007. *High temperature electrolyte supported Ni-GDC/YSZ/LSM SOFC operation on two-stage Viking gasifier product gas*. Journal of Power Sources 173, 357-366.

Koo K.Y., Lee S., Jung U.H., Roh H., Yoon W.L., 2014. *Syngas production via combined steam and carbon dioxide reforming of methane over Ni–Ce/*$MgAl_2O_4$ *catalysts with enhanced coke resistance*. Fuel Processing Technology 119, 115-157.

Lee W.Y., Hanna J., Ghoniem A.F., 2012. On the Predictions of Carbon Deposition on the Nickel Anode of a SOFC and Its Impact on Open-Circuit Conditions. Journal of the Electrochemical Society 160 (2), F94-F105.

Liu M., van der Kleij A., Verkooijen A.H.M., Aravind P.V., 2013. *An experimental study of the interaction between tar and SOFCs with Ni/GDC anodes*. Applied Energy 108, 149-157.

Lorente E., Berrueco C., Millan M., Brandon N.P., 2013. *Effects of tar fractions from coal gasification on nickel-yttria stabilized zirconia and nickel-gadolinium doped ceria solid oxide fuel cell anode materials.* Journal of Power Sources 242, 824-831.

Lorente E., Millan M., Brandon N.P., 2012. Use of gasification syngas in SOFC: Impact of real tar on anode materials. International Journal of Hydrogen Technology 37, 7271-7278.

Mermelstein J., Millan M., Brandon N., 2010. *The impact of steam and current density on carbon formation from biomass gasification tar on Ni/YSZ, and Ni/CGO solid oxide fuel cell anodes*. Journal of Power Sources 195, 1657-1666.

Mermelstein J., Millan M., Brandon N.P., 2011. *The interaction of biomass gasification syngas components with tar in a solid oxide fuel cell and operational conditions to mitigate carbon deposition on nickel-gadolinium doped ceria anodes*. Journal of Power Sources 196, 5027-5034.

Mermelstein J., Millan M., Brandon N.P., 2009. *The impact of carbon formation on Ni-YSZ anodes from biomass gasification model tars operating in dry conditions*. Chemical Engineering Science 64, 492-500.

Milne T. A.; Evans R. J.; Abatzoglou N., 1998. *Biomass gasifier "tars": Their nature, formation, and conversion*. Report NREL/TP-570-25357.

Namioka T., Naruse T., Yomane R., 2011. *Behaviour and mechanisms of Ni/ScSZ cermet anode deterioration by trace tar in wood gas in a solid oxide fuel cell*. International Journal of Hydrogen Energy 36, 5581-5588.

Singh D., Hernandez-Pacheco E., Hutton P.N., Patel N., Mann M.D., 2004. *Carbon deposition in an SOFC fueled by tar-laden biomass gas: a thermodynamic analysis*. Journal of Power Sources 142, 194-199.

Wang Y., Li F., Cheng H., Fan L., Zhao Y., 2013. *A comparative study on the catalytic properties of high Ni-loading Ni/SiO_2 and low Ni-loading Ni-Ce/SiO_2 for CO methanation*. Journal of Fuel Chemistry and Technology 41 (8), 972-977.

Zhu W.Z., Deevi S.C., 2003. *A review on the status of anode materials for solid oxide fuel cells*. Materials Science and Engineering A362, 228-239.